

# T-ray computed tomography

**Bradley Ferguson**

*Department of Physics, Applied Physics and Astronomy, Rensselaer Polytechnic Institute, Troy, New York 12180, Cooperative Research Centre for Sensor, Signal and Information Processing, Mawson Lakes, SA 5095, Australia, and Centre for Biomedical Engineering and Department of Electrical and Electronic Engineering, Adelaide University, SA 5005, Australia*

**Shaohong Wang**

*Department of Physics, Applied Physics and Astronomy, Rensselaer Polytechnic Institute, Troy, New York 12180*

**Doug Gray**

*Cooperative Research Centre for Sensor, Signal and Information Processing, Mawson Lakes, SA 5095, Australia*

**Derek Abbot**

*Centre for Biomedical Engineering and Department of Electrical and Electronic Engineering, Adelaide University, SA 5005, Australia*

**X.-C. Zhang**

*Department of Physics, Applied Physics and Astronomy, Rensselaer Polytechnic Institute, Troy, New York 12180*

Received January 28, 2002

We demonstrate a tomographic imaging modality that uses pulsed terahertz (THz) radiation to probe the optical properties of three-dimensional (3D) structures in the far-infrared. This THz-wave computed tomography (T-ray CT) system provides sectional images of objects in a manner analogous to conventional CT techniques such as x-ray CT. The transmitted amplitude and phase of broadband pulses of THz radiation are measured at multiple projection angles. The filtered backprojection algorithm is then used to reconstruct the target object, including both its 3D structure and its frequency-dependent far-infrared optical properties. © 2002 Optical Society of America

OCIS codes: 300.6270, 110.6880.

For just over a decade, terahertz (THz) time-domain spectroscopy has been used to determine the optical properties of materials in the submillimeter wavelength regime. More recently, two-dimensional (2D) THz imaging<sup>1-3</sup> has been demonstrated for a diverse range of applications, including imaging semiconductors, leaf moisture content, flames, skin burn severity, and skin cancer.<sup>4</sup> THz imaging is attractive for a number of reasons: The radiation is nonionizing and poses few safety risks, it is capable of submillimeter resolution, and, importantly, a number of materials, including paper, plastics, and cardboard, are relatively transparent in this frequency band. However, the three-dimensional (3D) structure of objects cannot be determined with conventional THz imaging techniques. In particular, the effects of variations in topography and the far-infrared optical properties of the sample have been indistinguishable.

A reflection-mode THz tomography system based on measuring the time of flight of reflected pulses was previously demonstrated.<sup>5</sup> This technique is capable of resolving the 3D refractive-index profiles of objects consisting of well-separated layers of differing refractive index. Although this technique provides extremely sensitive depth resolution of the order of 1  $\mu\text{m}$ , the current reconstruction algorithms are only applicable given a number of assumptions that restrict its applicability.<sup>4</sup> These algorithms neglect multiple reflections, absorption, and dispersion in the object to be imaged. These restrictions have motivated research into more-general tomographic imaging methodologies.

In this Letter we demonstrate the use of T-ray computed tomography (CT) for 3D imaging applications in the far-infrared. T-ray CT draws inspiration from the now ubiquitous x-ray CT system. Figure 1 shows a schematic of the T-ray CT system. The hardware is a relatively simple extension of modern transmission-mode THz imaging systems. The target sample is mounted on a rotation stage that allows it to be rotated, and a 2D THz image is obtained at each projection angle.

THz pulses are generated with a regeneratively amplified Ti:sapphire laser (Spectra Physics Hurricane) with an average output power of 700 mW, a center wavelength of 800 nm, a pulse duration of 130 fs, and a repetition rate of 1 kHz, incident upon a 14-mm-wide aperture photoconductive antenna with a bias of 2000 V. The THz radiation is focused by off-axis parabolic mirrors to a spot size of approximately 1 mm on the target. The transmitted THz pulse is collected with parabolic mirrors and focused onto a 4-mm-thick  $\langle 110 \rangle$  ZnTe electro-optic (EO) detector crystal.

The acquisition speed of the data is an important concern. We use a linearly chirped optical probe beam for EO detection of the THz pulses.<sup>3</sup> With this technique the full THz waveform is measured simultaneously, dramatically accelerating the imaging speed.

The optical probe pulse is linearly chirped and temporally stretched to a pulse width of 30 ps by use of a grating pair. The THz pulse modulates the probe pulse via the EO effect and is recovered with the spectrometer and a CCD camera. With a CCD exposure time of 50 ms, the signal-to-noise ratio for the system

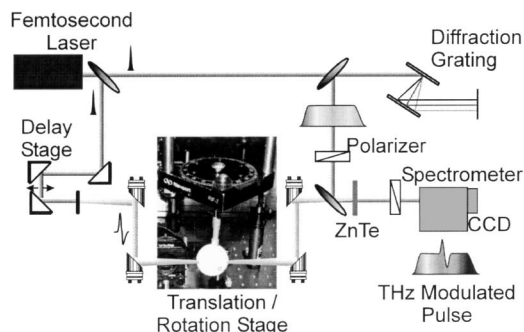


Fig. 1. Simplified hardware schematic used for T-ray CT. The ultrafast laser pulses are split into pump and probe beams. The pump beam triggers a biased (2000-V) wide-aperture antenna to generate THz pulses that are focused on the target by parabolic mirrors. The probe beam is linearly chirped by a grating pair to a pulse width of 30 ps. The THz temporal profile is encoded on the probe pulse by a 4-mm-thick ZnTe EO detector crystal and a pair of crossed polarizers. A spectrometer and a CCD camera are used to recover the THz signal. Inset, photograph of the rotation stage and sample. The sample is a dielectric sphere.

was approximately 100. The exposure time could be reduced to 5 ms at the expense of signal-to-noise ratio. The sample was mounted on an  $x$ - $y$  translation stage and raster scanned for image acquisition. The sample was then rotated, and the THz image was recorded at each projection angle.

This technique is still quite time consuming: A typical image of size  $100 \times 100$  pixels measured at 18 projection angles can take more than 1 h. Fortunately, this speed may be improved with alternative THz imaging techniques. Using 2D THz imaging with a CCD camera<sup>2</sup> may potentially reduce the acquisition time to less than a few minutes.

We used the filtered backprojection algorithm to perform an inverse Radon transform<sup>6</sup> to reconstruct the object of interest. The Radon transform is a line integral model, and in the present context this is equivalent to the approximation that the detected THz signal is simply related to the transmitted pulse by a line integral of the form

$$P_d(\omega, \theta, l) = P_t(\omega) \exp \left[ \int_{L(\theta, l)} \frac{-i\omega \hat{n}(x)}{c} dx \right], \quad (1)$$

where  $P_d$  is the Fourier transform of the detected THz signal at a frequency  $\omega$ , a projection angle  $\theta$ , and a horizontal offset from the axis of rotation,  $l$ .  $P_t$  is the Fourier component of the incident THz signal at the same frequency,  $L$  is the straight line between the source and detector, and  $\hat{n}(x) = n(x) + ik(x)$  is the unknown complex refractive index of the sample. If we consider the phase of the THz pulse in the time domain and additionally assume that we can neglect dispersion, this approximation is equivalent to assuming that  $\Delta t(\theta, l) = \int_{L(\theta, l)} n(x)/c dx$ , where  $\Delta t$  is the time difference between the peak of the THz pulse received if no sample is present and the pulse is measured for a given  $\theta$  and  $l$ .

The filtered backprojection algorithm is well known in x-ray CT. It is based on the Fourier slice theorem,<sup>7</sup>

which relates  $N(u, v)$ , the spatial 2D Fourier transform of the object function, and the Fourier transform of the parallel projection data,  $S(\theta, \omega)$ , defined as

$$S(\theta, \omega) = \int_{-\infty}^{\infty} s(\theta, l) \exp(-i2\pi\omega l) dl, \quad (2)$$

where  $\omega$  is the spatial frequency in the  $l$  direction.  $s(\theta, l)$  is extracted from the measured projection data. To reconstruct the refractive index of the sample with the time-domain data, we use  $s = \Delta t$ , and to perform the reconstruction for the absorption coefficient  $k(\omega)$  at a given frequency, we use  $s = \text{real}\{-\log[P_d(\omega)/P_t(\omega)]\}$ .

The filtered backprojection algorithm simply involves computing the Fourier transform of the projection data,  $S(\theta, \omega)$  for each angle, filtering this result with a Ram-Lak filter, and summing the inverse Fourier transforms of the filtered projections in the image ( $x, y$ ) plane. The filtered backprojection algorithm can be described by

$$\hat{n}(x, y) = \int_0^\pi \left[ \int_{-\infty}^{\infty} S(\theta, \omega) |\omega| \exp(i2\pi\omega l) d\omega \right] d\theta. \quad (3)$$

Unlike traditional x-ray CT, which measures only the amplitude of the transmitted radiation, T-ray CT measures the transmitted pulse shape. This allows more information about the sample to be recovered.

Figure 2(a) shows a vial containing a plastic tube that was imaged with the T-ray CT system. A coarse sampling step of 1 mm in the  $x$  and  $y$  dimensions was used to obtain projection images for each  $10^\circ$  angular increment. The coherent nature of pulsed THz systems was exploited, and the time of flight of the THz pulse for each projection was used to reconstruct the image shown in Fig. 2(b). The reconstructed image for one 2D cross section is shown. The intensity of the image is proportional to the reconstructed refractive index for each pixel, and the plastic tube can be seen to have a higher refractive index than the plastic vial wall. The mean refractive index of the center tube was found to be 1.52, which is in reasonable agreement with the refractive index of 1.58 determined with a normal THz time-domain spectroscopy system.

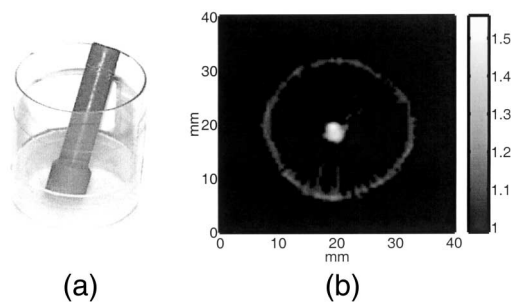


Fig. 2. A vial and plastic tube were used to test the T-ray CT system. (a) Optical image of the object. The timing of the peak of the pulse in the time domain was used as the input to the filtered backprojection algorithm and the cross section was reconstructed as shown in (b). Gray-scale intensity reflects the refractive index of the sample at each pixel; darker pixels correspond to a higher refractive index.

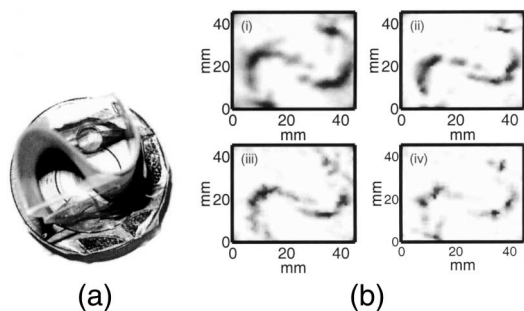


Fig. 3. A sheet of polyethylene was bent into an S shape and imaged with the T-ray CT system. (a) Optical image of the sample. The measured data were Fourier transformed, and the imaginary parts of the Fourier domain responses at four different frequencies were used to reconstruct the sample. (b) Reconstructed cross-sectional slices of the sample: (i) 0.2 THz, (ii) 0.4 THz, (iii) 0.6 THz, (iv) 0.8 THz.

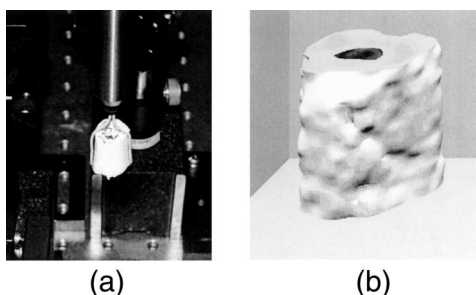


Fig. 4. A piece of turkey bone was imaged with the T-ray CT system. The fine structure inside the bone is of the order of the THz wavelength and therefore causes difficulties in reconstruction. (a) Optical image. The turkey bone was reconstructed, and (b) a 3D rendered image was generated. The reconstruction used the amplitude of the THz pulses at each pixel as the input to the filtered backprojection algorithm.

Because the vial wall is thinner than the reconstruction grid size, the refractive index is not recovered accurately. 2D THz imaging has been shown to have a resolution that is limited by the Rayleigh criterion to approximately 0.5 mm. Theoretically, a comparable resolution can be achieved with T-ray CT, provided that the data are sampled at enough projection angles that a fine enough reconstruction grid is ensured.

T-ray CT has the potential to identify targets based on their frequency response in the far-infrared. Figure 3(b) shows a reconstruction of the simple sample shown in Fig. 3(a) with the data from four different frequencies. The resolution of the reconstruction improves as the frequency increases, however, the signal-to-noise ratio decreases because most of the source power is at frequencies below 0.5 THz. Therefore, the reconstructions at higher frequencies suffer from additional artifacts caused by noise.

The filtered backprojection algorithm assumes that diffraction effects and Fresnel losses can be neglected.

This assumption works well for low-refractive-index targets with features that are large relative to the wavelength of the THz radiation (0.3 mm at 1 THz); however, for more-complex targets with fine structure the filtered backprojection algorithm is unable to reconstruct the target accurately. Figure 4(a) shows an optical photograph of a more-complex target: a piece of turkey bone. This sample was imaged with the T-ray CT system, and the amplitude of the measured THz pulses was used to reconstruct the bone. The reconstructed slices were then 3D rendered to generate the image shown in Fig. 4(b). It is obvious that, although the outer profile was reconstructed with reasonable accuracy, the fine internal structure was not recovered.

This technique extends the potential of THz time-domain spectroscopy to several exciting new application areas. It is capable of reconstructing the 3D structure and the far-infrared optical properties of an object. The images may potentially be obtained relatively quickly with the aid of 2D THz imaging with a CCD camera.<sup>8</sup> Importantly, by use of the frequency-dependent complex refractive index, different materials may be uniquely identified despite being hidden within other opaque structures. We foresee applications of this technique in nondestructive mail and packaging inspection, semiconductor testing, and manufacturing quality control.

This work was supported in part by the U.S. Army Research Office, and the Center for Subsurface Sensing and Imaging Systems, under the Engineering Research Centers Program of the U.S. National Science Foundation. B. Ferguson thanks the Australian-American Fulbright Commission and the Australian Research Council. Discussions with Wang Li are also gratefully acknowledged. X.-C. Zhang's e-mail address is zhangxc@rpi.edu.

## References

1. B. B. Hu and M. C. Nuss, *Opt. Lett.* **20**, 1716 (1995).
2. Q. Wu, T. D. Hewitt, and X.-C. Zhang, *Appl. Phys. Lett.* **69**, 1026 (1996).
3. Z. Jiang and X.-C. Zhang, *Appl. Phys. Lett.* **72**, 1945 (1998).
4. D. M. Mittleman, M. Gupta, R. Neelamani, R. G. Baraniuk, J. V. Rudd, and M. Koch, *Appl. Phys. B* **68**, 1085 (1999).
5. D. M. Mittleman, S. Hunsche, L. Boivin, and M. C. Nuss, *Opt. Lett.* **22**, 904 (1997).
6. G. T. Herman, *Image Reconstruction From Projections—The Fundamentals of Computerized Tomography* (Academic, New York, 1980).
7. A. C. Kak and M. Slaney, *Principles of Computerized Tomographic Imaging* (Society for Industrial and Applied Mathematics, Philadelphia, Pa., 2001).
8. B. Ferguson, S. Wang, D. Gray, D. Abbott, and X.-C. Zhang, in *Thirteenth International Conference on Ultrafast Phenomena*, (Optical Society of America, Washington, D.C., 2002), pp. 450–451.